ADVANCES IN ATMOSPHERIC SCIENCES, VOL. 30, NO. 6, 2013, 1526–1534

Examination of the Quality of GOSAT/CAI Cloud Flag Data over Beijing Using Ground-based Cloud Data

HUO Juan*(霍 娟), ZHANG Wenxing (章文星), ZENG Xiaoxia (曾晓夏),
LÜ Daren (吕达仁), and LIU Yi (刘 毅)

Key Laboratory for Atmosphere and Global Environment Observation, Institute of Atmospheric Physics, Chinese Academy of Sciences, Beijing 100029

(Received 25 October 2012; revised 20 February 2013; accepted 22 February 2013)

ABSTRACT

It has been several years since the Greenhouse Gases Observing Satellite (GOSAT) began to observe the distribution of CO_2 and CH_4 over the globe from space. Results from Thermal and Near-infrared Sensor for Carbon Observation-Cloud and Aerosol Imager (TANSO-CAI) cloud screening are necessary for the retrieval of CO_2 and CH_4 gas concentrations for GOSAT TANSO-Fourier Transform Spectrometer (FTS) observations. In this study, TANSO-CAI cloud flag data were compared with ground-based cloud data collected by an all-sky imager (ASI) over Beijing from June 2009 to May 2012 to examine the data quality. The results showed that the CAI has an obvious cloudy tendency bias over Beijing, especially in winter. The main reason might be that heavy aerosols in the sky are incorrectly determined as cloudy pixels by the CAI algorithm. Results also showed that the CAI algorithm sometimes neglects some high thin cirrus cloud over this area.

Key words: Greenhouse Gases Observing Satellite, Thermal and Near-infrared Sensor for Carbon Observation-Cloud and Aerosol Imager, all-sky imager, cloud

Citation: Huo, J., W. X. Zhang, X. X. Zeng, D. R. Lü, and Y. Liu, 2013: Examination of the quality of GOSAT/CAI cloud flag data over Beijing using ground-based cloud data. *Adv. Atmos. Sci.*, **30**(6), 1526–1534, doi: 10.1007/s00376-013-2267-0.

1. Introduction

The main reason behind the current issue of global warming is the increases of CO_2 and CH_4, both products of the development of modern industry and civilization (Fan et al., 1998; Bousquet et al., 2000; Treut et al., 2007). Observations of these greenhouse gases are vital for understanding carbon cycle mechanisms and predicting global climate change through General Circulation Models (GCMs) (Fan et al., 1998). The Greenhouse Gases Observing Satellite (GOSAT), developed by the Japan Aerospace Exploration Agency (JAXA), Ministry of the Environment (MOE) and the National Institute for Environmental Studies (NIES) in Japan, was launched in January 2009 in order to observe greenhouse gases (CO_2 and CH_4, mainly) over the whole globe (http://www.gosat.nies.go.jp). Remote sensing by instruments onboard satellites, different from and superior to "traditional" observations (i.e. sampling and measuring the concentration of gases), allows both the temporal variation and spatial distribution of greenhouse gases to be monitored, including in isolated and sparsely populated areas, and the upper atmosphere, which are otherwise very difficult to observe (Engelen et al., 2001).

GOSAT is a sun-synchronous satellite operating at an altitude of approximately 666 km and is equipped with two instruments: a Fourier Transform Spectrometer (FTS) and a Cloud and Aerosol Imager (CAI). The FTS observes high-resolution spectroscopic near-infrared sunlight reflected from the ground during daytime and thermal radiation from the Earth's surface and atmosphere during daytime and nighttime. The information obtained by the FTS is used to derive the radiation of molecular absorption, i.e. the 2.0-μm CO_2 absorption range, 1.6-μm CO_2 and/or CH_4 absorption

*Corresponding author: HUO Juan, huojuan@mail.iap.ac.cn

range, as well as thermal infrared range. The radiation is then used to retrieve gas concentrations in the atmosphere and their vertical profiles. In fact, in addition to the impact of gases in the atmosphere, the radiation obtained by the FTS will also be influenced by clouds, aerosols and the albedo of the Earth's surface. Radiation data contaminated by clouds and/or aerosols should be excluded or further processed for the precise estimation of gas (CO_2/CH_4) concentrations. Supplementary to the FTS, the CAI is a sensor that observes and acquires information on aerosols and clouds.

The CAI is a multichannel, narrow-band passive imager that captures an "image" of the atmosphere and ground during the daytime, covering the area observed by the FTS, from ultraviolet to near-infrared wavelengths. Its spatial resolution in nadir view, with an observation scan width of about 1000 km, is about 500 m for bands 1 through 3, and about 1500 m for band 4 with a 750 km scan width. The center wavelengths of bands 1, 2, 3 and 4 are 0.38, 0.68, 0.87 and 1.6 μm, respectively. When CAI data detect aerosols, cirrus cloud or dense cloud in the view of the FTS, FTS data should be discarded (for cloudy conditions) or be corrected (for aerosols) depending on the information derived from the CAI.

The cloud data processing algorithm used by the CAI is the Cloud and Aerosol Unbiased Decision Intellectual Algorithm (CLAUDIA), which is applied for clear-sky and cloud detection (Ishida and Nakjima, 2009). CLAUDIA comprises multiple threshold tests and threshold values according to water, land, the polar region etc., which have different spectral radiances reflected from clouds, aerosols and the ground. CLAUDIA is considered a neutral algorithm, which means that the degrees of ambiguity of cloud determination are provided and the results of cloud detection are not biased to either cloudy or clear conditions. Based on CLAUDIA, the CAI level-2 cloud flag data products released by GOSAT are provided as clear-sky confidence levels (CCLs, also referred to as Q hereinafter, ranging between 0.0 and 1.0), which are divided into 16 levels with 15 thresholds (0.94, 0.88, 0.82, 0.76, 0.7, 0.64, 0.58, 0.52, 0.46, 0.4, 0.34, 0.28, 0.22, 0.16 and 0.1) and stored for each pixel taken by the CAI. The Q value provides the basic information to determine cloud flags. For the CAI, pixels with $Q<0.1$ are categorized as cloudy, pixels with $0.1\leqslant Q\leqslant 0.94$ are grouped as ambiguous, and pixels with $0.94<Q\leqslant 1$ are regarded as clear. Ishida and Nakjima (2011) investigated CAI cloud determination ability through comparison with Aqua/MODIS cloud data, which were considered as providing true values in their analysis. They analyzed four months of data respectively chosen from four seasons from 2009 to 2010 over the whole globe and found that the CAI data were mostly in good agreement with MODIS over water, whereas sometimes provided a cloudy tendency over land. In the present reported study, we made another comparison between CAI cloud screening data and ground-based cloud data, but for the period 2009–2012, and over an urban area (Beijing).

In section 2, basic information about the two ground-based observation instruments (visible all-sky imager and scanning infrared imaging system) is presented. In section 3, an illustration of the method used for the comparison between CAI- and ground-based cloud data is provided. The results, including a statistical analysis and two typical cases, are described in section 4. And finally, a discussion and summary of the findings are presented in section 5.

2. Ground-based observations

2.1 *All-sky imager*

The all-sky imager (ASI) used was developed by the Institute of Atmospheric Physics, Chinese Academy of Sciences (Huo and Lu, 2009). It has a digital camera equipped with a fish-eye lens that captures visible all-sky images in color at a resolution of 4288×2848. The ASI is also equipped with a device that obscures direct solar light and protects the sensor from damage. As is known, atmospheric molecular Rayleigh scattering, different from Mie scattering (i.e. cloud scattering), which is almost independent of wavelength, is wavelength (λ) dependent ($\propto \lambda^{-4}$). Therefore, blue light is scattered more than red light in clear skies, whereas clouds approximately scatter the red and blue light equally (Sabburg and Long, 2004).

Fig. 1. The ASI (circled) and SIRIS (highlighted in a rectangle) located on the office building of the Institute of Atmospheric Physics, Chinese Academy of Sciences.

This is the reason why clouds appear white and clear sky appears blue to the human eye. The ratio of blue to red light is then used by the ASI to discriminate cloud from sky. The ASI has a cloud determination algorithm that uses adaptive thresholds to discriminate each cloudy or clear pixel on an all-sky image (Huo and Lu, 2009). Figure 1 shows the ASI (circled) located on the roof of our office building at the Institute of Atmospheric Physics (116.37°N, 39.97°E). It works during both day- and nighttime, capturing an image every three minutes.

2.2 *Scanning infrared imaging system*

The scanning and infrared imaging system (SIRIS), also developed by the Institute of Atmospheric Physics, obtains thermal infrared (8–12 μm) all-sky brightness temperature through a scan mode (Zhang et al., 2007). Thermal radiation (also described as brightness temperature) from the sky obtained by SIRIS is composed of thermal emission/absorption radiation from gases (i.e. vapor) contained in the atmosphere and cloud (if it exists). In general, thermal infrared brightness temperature (TB hereinafter) from clear sky, which is mostly affected by the vapor and temperature going through the observation path, can be estimated by a radiative transfer model when the normal atmospheric properties of vertical profiles have been known before. Clouds have stronger thermal emission radiation and most cloud, except very thin cloud, can be considered as a black body, which means that TB obtained by SIRIS can be considered as thermal radiation emitted from the bottom of clouds. Therefore, TB from clouds is generally higher than that from clear sky and is related to cloud-bottom height, because the temperature of the atmosphere decreases with increasing altitude. SIRIS is now capable of detecting most cloud types, except very thin cloud, and estimating the base height of clouds. For skies with heavy aerosols, dust and fog, SIRIS shows better ability in detecting cloud than the ASI because those factors will change the visible scattering characteristics of clear sky and reduce the difference between clouds, while they have little impact on thermal infrared radiation of both non-cloudy and cloudy skies. However, the temporal and spatial resolution of SIRIS is lower than for the ASI since it works by a mechanical scanning mode (it needs at least five minutes to finish a whole-sky scanning). It scans (every 15 minutes) in only 4023 directions across the whole sky. Figure 1 shows SIRIS (highlighted in a rectangle) located about 2 m from the ASI on the roof of our office building. SIRIS and the ASI have worked together simultaneously for more than six years since 2006. The TB data from SIRIS, combined with ASI images, are used to classify the sky into three categories: clear, cloudy, and overcast.

3. Comparison method

We investigated the ability of CAI cloud detection over an urban area through comparison with ASI cloud data. GOSAT passes across our office building (116.37°N, 39.97°E) at around 0528 UTC every three days. ASI and SIRIS images that were taken at the closest time to CAI observations were chosen from 1 June 2009 to 1 May 2012 for comparison.

Since the ASI has a fish-eye lens with a 180° field of view, each image is captured by equi-angle projection, and not by geometric projection. This means that each pixel of the image contains the zenith and azimuth information of the incidence light, but not the geometric information. For instance, a pixel in the center of an ASI (circular) image is the zenith, meaning its zenith angle is 0° and azimuth angle is 0°–360°, while pixels on the edge have the same zenith angle of 90° and their azimuth angles are 0°–360° (Fig. 2). SIRIS has the same projection mode as the ASI. The radius (R)

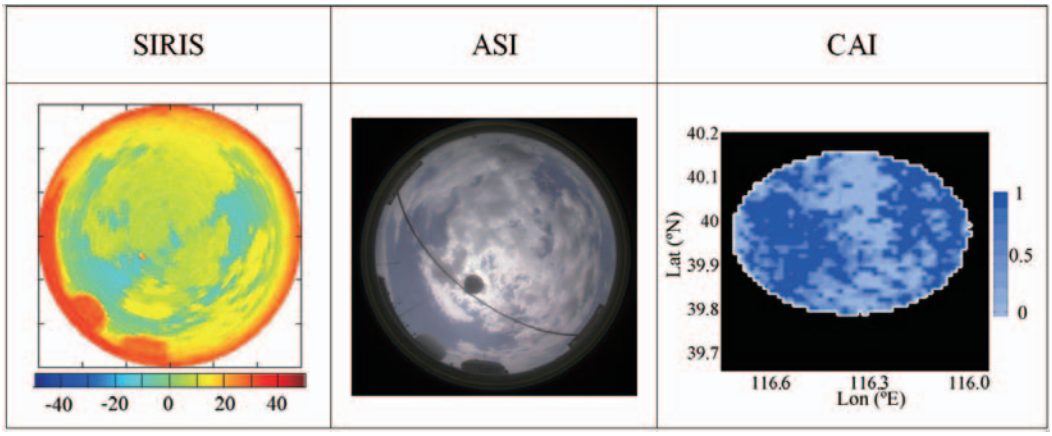

Fig. 2. Samples of SIRIS, ASI and CAI images obtained respectively at 1330, 1327 and 1326 LST 30 May 2010.

of the area observed by the ASI can be calculated as

$$R = H\mathrm{tg}\Theta\,, \tag{1}$$

where Θ is the zenith angle and H is the height of the object (i.e. cloud). Then, the observation radius (R) is about 15 km when H (base-height of cloud) is 4 km and Θ is 75°. According to the abovementioned principle of classifying CAI data, pixels that clear the confidence level of Q<0.1 are considered cloudy, while pixels with $Q\geqslant$0.94 are regarded as clear and pixels with 0.1$\leqslant Q<$0.94 are ambiguous. We used this same threshold to classify the pixels of CAI data products into three groups: clear, cloudy and ambiguous. Using the base-height of cloud retrieved from SIRIS, we were able to estimate the approximate radius of the area that the ASI observes, meaning we could then select the CAI cloud flag data pixels within this area to produce a false-color "CAI image" (Fig. 2, right panel; pure blue represents "clear"; white represents "cloudy"; while other blue colors with different shades of gray represent ambiguous pixels with different Q values). Three samples from SIRIS, ASI and CAI, taken at 1330, 1327 and 1326 LST 30 May 2010, respectively, are shown in Fig. 2. In order to exclude buildings that partially obscure the sky near the horizon, we only used pixels for which the zenith angle was less than 75°. The radius of the region for comparison was 20 km for clear sky since there were no clouds in the sky, and for an area with this size radius, the CAI image consisted of about 4900 pixels. As described above, pixels with different zenith angles on the ASI images had different spatial resolutions, which were dependent on the cloud height. Obviously, it is hard to make a point-to-point comparison between ASI cloud data and CAI cloud flag data since each piece of CAI cloud flag data contains latitude and longitude information and the spatial resolution varies with view angle. To illustrate the comparisons clearly, we categorized the matched image data into three groups: (1) those where both ASI and SIRIS data illustrated that the sky was overcast before and after the time of the CAI observation (namely, cloud cover was ten tenths at least 15 minutes before and after the acquisition time of the CAI data); (2) those where both ASI and SIRIS data illustrated that the sky was clear (namely, cloud cover was zero tenths at least 15 minutes before and after the acquisition time of the CAI data); and (3) those indicating cases that could be regarded as partially cloudy.

4. Statistical analysis and comparison results

GOSAT passes over our office building every three days at roughly the same time (approximately 1330 LST). CAI data were unavailable for February 2011 to May 2011 because of problems with the instrument, and the ASI and SIRIS also failed to work on occasions. Taking this downtime into account, there were a total of 236 matched cases/images available for comparison during the period 1 June 2009 to 1 May 2012, considering that matched cases should have almost the same observation area and time.

Table 1. Numbers of cases of each category (clear, cloudy, overcast) distributed throughout the four seasons.

	Overcast	Cloudy	Clear
Spring	12	28	10
Summer	22	32	6
Autumn	14	18	23
Winter	7	24	40

We extracted 55 overcast images (images full of cloud), 79 clear images (no cloud at all), and 102 partially cloudy (referred to simply as "cloudy") images through examining each ASI and SIRIS image through a manual inspection process before and after the matched observation time. Table 1 shows the numbers of cases distributed across the four seasons. For winter, the least amount 7 was for overcast cases, while the largest 40 was for clear cases. On the contrary, for summer the largest amount 32 was for overcast cases and the least 6 was for clear cases. This distribution is in accordance with the characteristic climate of Beijing, which has a temperate sub-humid continental monsoon climate, i.e. summer is hot and humid whereas winter is cold and dry. The selection can be regarded as semi-random because cases were chosen according to ASI and CAI observation times (once every three days, usually). Therefore, the analysis based on these cases can be considered as representative.

4.1 *Overcast sky*

Overcast sky here means sky that was full of cloud in the observation field view. In other words, all the pixels on the CAI image within the area were "cloudy"; that is, Q<0.1. For the 55 overcast images, CAI estimated 29 as overcast and 26 images as partially cloudy, meaning these skies consisted of cloudy, clear and ambiguous pixels. About 94.7%, 5% and 0.3% of the CAI pixels were recorded as cloudy, ambiguous and clear, respectively. The CAI showed very good agreement with the ASI for overcast sky. The histogram shown in Fig. 3a illustrates the ratio of the number of each category in the four seasons to the number of total pixels. It can be seen that the maximum number pixels for which wrong identifications were made occurred in summer (about 11.2% pixels were regarded as ambiguous and clear), whereas spring had the minimum

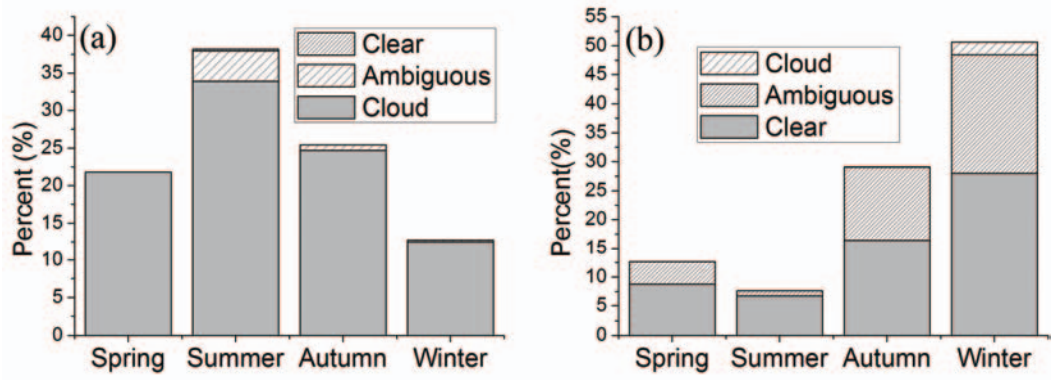

Fig. 3. Distribution of clear, ambiguous and cloudy pixels from CAI cloud flag data across the four seasons when ASI images showed (a) skies were overcast and (b) all skies were totally clear. The y-axis is the ratio (%) of the number of pixels in each category (clear, ambiguous and cloudy) in a season to the number of all pixels across all four seasons.

(about 1.9% pixels were not regarded as cloudy). The average value of Q ($1 \geqslant Q \geqslant 0.1$; namely, not cloudy) of CAI pixels was 0.217 and the standard deviation was 0.093. CAI identified most pixels as cloudy for these overcast skies, but there were some pixels regarded wrongly as clear and ambiguous, although their average Q value was not high.

4.2 *Clear sky*

Clear sky here refers to no cloud at all in the observation field view, and since there is no cloud in such cases, there is also no cloud-base height. We selected CAI pixels within a 20-km radius for our examination. In this region, the Q value of all pixels according to the CAI should not be less than 0.94 to be classed as "clear".

There were 79 ASI clear-sky cases, but each matched CAI image had cloudy pixels on it. About 59.87%, 37.86% and 2.27% of the CAI pixels were recorded as clear, ambiguous, and cloudy, respectively, for all clear cases. Obviously, the CAI identified many more clear pixels as cloudy and ambiguous than cloudy pixels as clear (described above). The histogram shown in Fig. 3b illustrates the distribution of the three categories across the four seasons. Winter showed the maximum number pixels (about 44.56% of all pixels in winter) regarded as ambiguous/cloudy, whereas summer showed the minimum (about 12.03% of all pixels in summer). More clear pixels were regarded as cloudy or ambiguous in winter than in summer. The reason might be related to the different cloud types and aerosols distributed in summer and winter. On the one hand, the mean optical depth of clouds that occur in summer is often higher than in winter, and skies with one layer of thin cirrus cloud occur more often in winter than in other seasons over Beijing owing to the temperate sub-humid continental monsoon climate (Liu et al., 2003; Min et al., 2011). On the other hand, studies have shown that the average aerosol optical depth (AOD) over Beijing was above 0.4 from the year 2000 to 2009, and had an increasing trend during that period (Xu et al., 2009; Yan and Liu, 2009; Guan and Li, 2010). At present, CLAUDIA only uses the radiances of three bands (with center wavelengths of 0.68, 0.87 and 1.4 μm) and their ratios to calculate the Q value. Since heavy aerosols and thin cloud have almost similar scattering characteristics for the three bands under certain conditions, CLAUDIA is currently not entirely efficient at identifying aerosols from thin cloud, especially when the AOD is high. In winter, thin clouds and more aerosols suspended in the atmosphere enhance the complexity of pixel discrimination. Thus, impacts from both thin clouds and aerosols cause more clear pixels to be identified as cloudy or ambiguous in winter than in summer. The bias of identification changed little if we set the threshold of Q to be lower for "clear"; for instance, if we regarded pixels with $Q \geqslant 0.88$ as clear, then the statistical percentage of clear, ambiguous and cloudy pixels to all pixels was 60.1%, 37.7% and 2.2%, respectively. If we regarded pixel with $Q \geqslant 0.52$ as clear, then the statistical percentage of clear, ambiguous and cloudy pixels to all pixels was 75.9%, 21.9% and 2.2%, respectively. The average value of Q of all pixels ($0 \leqslant Q < 0.94$) was 0.54 and the standard deviation 0.12. For all those clear pixels, the final average Q value from CAI data was much lower than 0.94, implying that CAI tends to identify clear pixels as cloudy over Beijing, a property also revealed by Ishida and Nakjima (2011). However, our analysis shows that the bias of CAI cloud screening for "cloudy" is much greater over Beijing, reaching about 40%, and the percentage of misidentification as cloud is greater than 50% due to aerosol pollution.

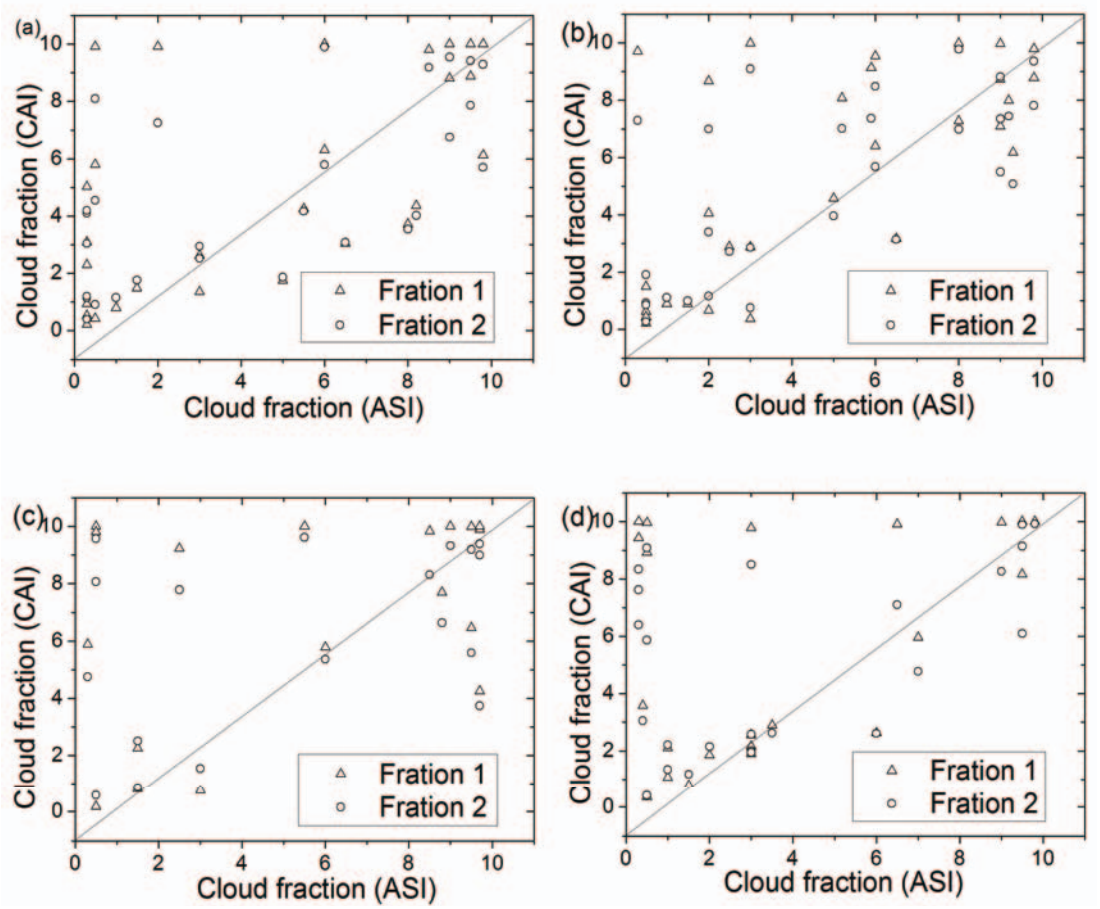

Fig. 4. ASI and CAI cloud fractions across the four seasons: (a) spring; (b) summer; (c) autumn; (d) winter. Fraction 1 is the ratio of the number of pixels (Q<0.52) regarded as cloudy to all pixels. Fraction 2 is the mean value of 1–Q of all pixels.

4.3 *Cloudy sky*

As mentioned above, a point-to-point comparison between the ASI and CAI is hard to perform because of different spatial resolutions and projection modes. The Q value of CAI data indicates the level of certainty in identifying clear or cloudy pixels, and thus may be regarded as the possibility that cloudy or clear pixels occur in a particular area, which can then be used to estimate the cloud fraction over that region. In this section, we compare CAI with ASI having used them to estimate the cloud fraction for the same area. For CAI, cloud fraction was estimated through two methods. The first (fraction 1) was the ratio of the number of pixels with Q<0.52 (not <0.94), which were regarded as cloudy, to all pixels, considering that the CAI has a cloudy tendency. The second (fraction 2) was the mean value of 1–Q of all pixels, used as a reference for fraction 1. The cloud fraction of the ASI (F_a) was the ratio of the number of pixels determined as cloud to the number of all pixels. Figure 4 shows ASI and CAI cloud fractions across the four seasons (cloud fraction expressed in tenths). When F_a was less than two tenths, both fraction 1 and fraction 2 were greater than F_a, especially for winter (Fig. 4d) and spring (Fig. 4a), which again verifies that the CAI (through CLAUDIA) identifies more pixels as cloudy pixels than the ASI. The Pearson correlation coefficient between F_a and fraction 1 was 0.51 and −0.14 for cases where F_a was greater than two tenths and not greater than two tenths, respectively. When F_a was greater than two tenths, cloud fractions of CAI showed good agreement with F_a in all four seasons, considering the movement of cloud as well as the spatial resolution. However, there were more cases where fraction 1 or fraction 2 was greater than F_a. A comparison of cloudy cases across all four seasons also showed the CAI cloudy bias.

4.4 *Comparison of two typical cases*

Here we detail two cases in which the CAI made different identifications to those captured by the ASI.

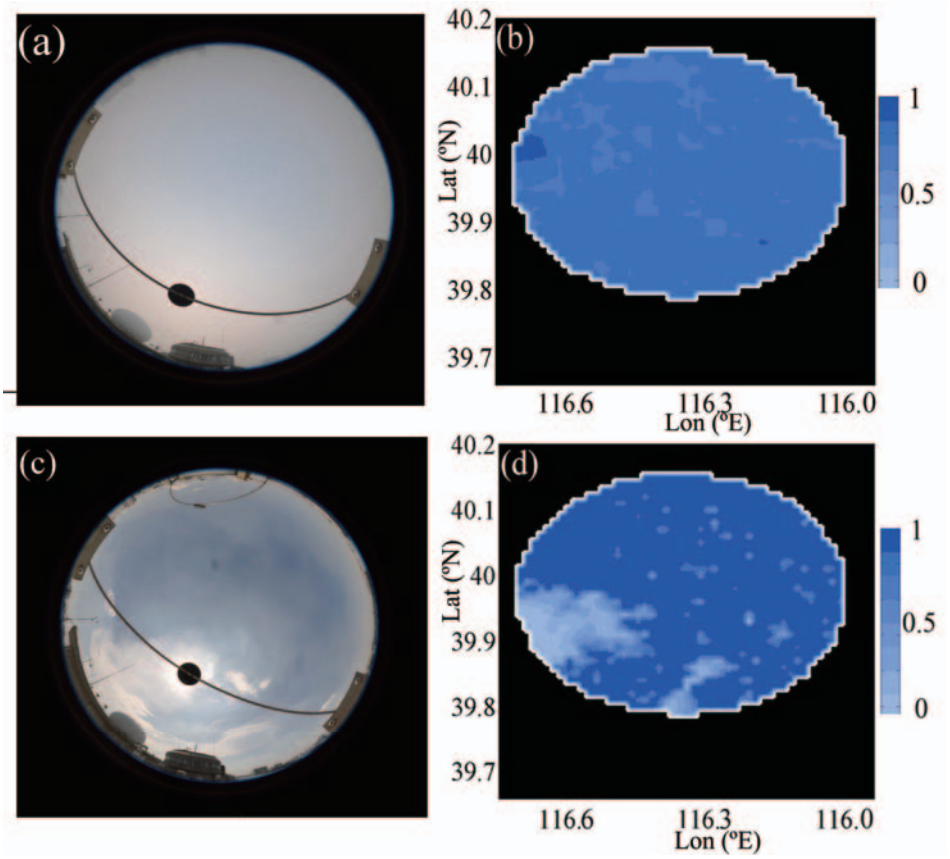

Fig. 5. Two comparative cases from ASI and CAI data. (a) ASI image, showing haze and fog, taken at 1328 LST 9 October 2010. (b) False-colored CAI image taken at 0527 UTC 9 October 2010. (c) ASI image, showing thin cirrus cloud, taken at 1327 LST 16 August 2010. (d) False-colored CAI image taken at 0526 UTC 16 August 2010.

Figure 5a illustrates an ASI image, containing heavy haze and fog, taken at 1328 LST 9 October 2010. This non-cloudy sky looks whiter (even yellow) than ordinary clear sky because of the haze and fog. Figure 5b shows a false-colored CAI image produced from cloud flag data. About 99% of pixels with $Q<0.94$ were regarded as cloudy and ambiguous by the CAI, whereas the real sky was contaminated by aerosols and fog, without cloud. The impacts from both aerosols and vapor thus challenge the ability of CAI cloud screening. Figure 5c shows an image taken at 1327 LST 16 August 2010 by the ASI. It can be seen that there were two layers of cloud in the sky: one lower fractocumulus cloud layer, and another higher thin-cirrus cloud layer. The mean base-height of the cirrus cloud was about 9 km. About 77.8% of the pixels of the CAI cloud flag data ($Q\geqslant 0.94$) were incorrectly regarded as clear, and 17.9% of the pixels were recorded as ambiguous. The CAI detected some cloudy pixels, but did not find all of the cirrus cloud because it was too thin to be noticed by the human eye.

The cases described above can certainly be regarded as typical cases, as other similar situations were found on different occasions. These cases and the associated analysis suggest that thin cloud and heavy aerosols sometimes tend to be confused by CLAUDIA, highlighting the need for this algorithm used by CAI cloud screening to be further improved to help address this issue in the future.

5. Summary and discussion

We analyzed CAI cloud screening data through comparison with ASI data over Beijing. We found that the CAI has a strong tendency for cloudy/clear identification over Beijing, especially in winter and autumn. On the other hand, the CAI sometimes tends to miss thin cirrus cloud. Comparisons between the four seasons showed that the reflectance of land over Beijing might not be the main source of the uncertainty.

Rather, it might be the haze (or fog) distributed in the lower atmosphere that confuses the algorithm of the CAI for cloud screening.

As mentioned above, the CAI is a passive imager that captures integrated radiation from the atmosphere and ground. The center wavelengths of channels 1, 2, 3 and 4 are 0.38, 0.68, 0.87 and 1.6 μm, respectively. Channels 2–4 are assigned to estimate the properties of clouds and aerosols. Parameters of clouds and aerosols, such as type, concentration and particle size, challenge the ability of the CAI. In general, a combination of channels 2–4 is efficient for discriminating between cloud and aerosol when the quantity magnitude of the concentration of cloud particles apparently differentiates from aerosol, which often exists in a relatively pure atmosphere where the effect of aerosol can be neglected. However, as the scattering properties of cloud and aerosol are similar in these three channels, it is difficult for the CAI to thoroughly discriminate between them because the radiation acquired by the CAI is an integrated value containing information from the atmospheric column with complex and various distributions of cloud and aerosol, especially heavy aerosol. For other instruments onboard passive sensing satellites, such as MODIS, more spectral channels are used to retrieve cloud mask data and reduce the level of uncertainty (Ackerman et al., 1998).

Some new processing methods might be suitable for enhancing the ability of the present algorithm. CLAUDIA applies a "minimum albedo" map, which is obtained from the minimum albedo of every band one month before the data acquisition date, as a clear identification rule for multiple thresholding. It is based on an assumption that clear conditions must exist within a certain region at least once per month, and the minimum albedo must be the reflectance of the Earth's surface. However, in reality nature is not this uniform, especially for areas where the AOD is relatively high and always varies with time. The minimum albedo sometimes contains reflectance from aerosols, which is not good for the identification of thin cloud, and sometimes the minimum albedo should be increased to avoid impacts from fog and aerosol. Discrimination of aerosol (haze) and thin cirrus cloud need to be emphasized in future work to improve the CAI cloud-screening algorithm. Applying more radiative information observed from other wavelength bands, i.e. from FTS, into the algorithm might be efficient. In addition, simulation of upward radiation by a radiative transfer model over a certain area can be used as a reference to produce and find the exact "minimum albedo" map. Feature analysis, e.g. the wavelet analysis, of the image within a certain area also helps to discriminate the "object" from "background". Further work along these lines will be performed by our group in the future.

Acknowledgements. The authors acknowledge support from the Strategic Pilot Science and Technology project of the Chinese Academy of Sciences (Grant No. XDA05040200) and the National Natural Science Foundation of China (Grant No. 41275040).

REFERENCES

Ackerman, S. A., K. I. Strabala, W. P. Menzel, R. A. Frey, C. C. Moeller, and L. E. Gumley, 1998: Discriminating clear-sky from clouds with MODIS. *J. Geophys. Res.*, **103**, 32141–32157.

Bousquet, P., P. Peylin, P. Ciais, C. L. Quere, P. Friedlingstein, and P. P. Tans, 2000: Regional changes in carbon dioxide fluxes of land and oceans since 1980. *Science*, **290**(5495), 1342–1346.

Engelen, R. J., A. S. Denning, K. R. Gurney, and G. L. Stephens, 2001: Global observations of the carbon budget: 1. Expected satellite capabilities for emission spectroscopy in the EOS and NPOESS eras. *J. Geophys. Res.*, **106**(D17), 20055–20068.

Fan, S., M. Gloor, J. Mahlman, S. Pacala, J. Sarmiento, T. Takahashi, and A. P. Tans, 1998: A large terrestrial carbon sink in North America implied by atmospheric and oceanic carbon dioxide data and models. *Science*, **282**(5388), 442–446.

Guan, J. X., and C. C. Li, 2010: Spatial distributions and changes of aerosol optical depth over eastern and central china. *Acta Scientiarum Naturalium Universitatis Pekinensis* , **46**, 185–191. (in Chinese)

Huo, J., and D. Lu, 2009: Cloud determination of all-sky images under low-visibility conditions. *J. Atmos. Ocean. Technol.*, **26**, 2172–2181.

Ishida, H., and T. Y. Nakjima, 2009: Development of an unbiased cloud detection algorithm for a spaceborne multispectral imager. *J. Geophys. Res.*, **114**, D07206, doi: 07210.01029/02008JD010710.

Ishida, H., and T. Y. Nakjima, 2011: Investigation of GOSAT TANSO-CAI cloud screening ability through an intersatellite comparison. *J. Appl. Meteor. Climatol.*, **50**, 1571–1586.

Liu, H., W. Zhu, S. Yi, W. Li, L. Chen, and L. Bai, 2003: Climatic analysis of the cloud over China. *Acta Meteorologica Sinica*, **61**, 466–473. (in Chinese)

Min, M., P. Wang, and X. Zong, 2011: Cirrus cloud distribution over China from spaceborne lidar observations. *Climatic and Environmental Research*, **16**, 301–309. (in Chinese)

Sabburg, J., and C. Long, 2004: Improved sky imaging for studies of enhanced UV irradiance. *Atmos. Chem. Phys*, **4**, 2543–2552.

Treut, L., R. Somerville, U. Cubasch, Y. Ding, C. Mauritzen, A. Mokssit, T. Peterson, and M. Prather, 2007: Historical overview of climate change. *Climate Change 2007: The Physical Science Basis. Contribu-*

tion of Working Group I to the Fourth Assessment report of the Intergovernmental Panel on Climate Change, Cambridge University Press, 996pp.

Xu, X., J. Qiu, S. Niu, and L. Tang, 2009. Optical depth of the atmospheric aerosol at 12 stations in China over the past 45 years. *Acta Scientiae Circumstantiae*, **29**, 488–495. (in Chinese)

Yan, L. B., and X. D. Liu, 2009: Seasonal variation of atmospheric aerosol and its relation to cloud faction over Beijing-Tianjin-Hebei region. *Chinese Research of Environmental Sciences*, **22**, 924–931. (in Chinese)

Zhang, W., D. Lu, and Y. Chang, 2007: A feasibility study of cloud base height remote sensing by simulating ground-based thermal infrared brightness temperature measurements. *Chinese Journal of Geophysics*, **50**, 339–350. (in Chinese)